

# Dynamical regimes of a quantum swap gate beyond the Fermi Golden Rule.

Axel D. Dente, Raúl A. Bustos-Marín and Horacio M. Pastawski

*Facultad de Matemática, Astronomía y Física,  
and Instituto de Física (CONICET), Universidad Nacional de Córdoba,  
Ciudad Universitaria, 5000 Córdoba, Argentina*

We discuss how the bath's memory affects the dynamics of a swap gate. We present an exactly solvable model that shows various dynamical transitions when treated beyond the Fermi Golden Rule. By moving continuously a single parameter, the unperturbed Rabi frequency, we sweep through different analytic properties of the density of states: I) collapsed resonances that split at an exceptional point in II) two resolved resonances ; III) out-of-band resonances; IV) virtual states; and V) pure point spectrum. We associate them with distinctive dynamical regimes: overdamped, damped oscillations, environment controlled quantum diffusion, anomalous diffusion and localized dynamics respectively. The frequency of the swap gate depends differently on the unperturbed Rabi frequency. In region I) there is no oscillation at all, while in the regions III) and IV) the oscillation frequency is particularly stable because it is determined by environment's band width. The anomalous diffusion could be used as a signature for the presence of the elusive virtual states.

## I. INTRODUCTION

It is well known that processing information using quantum mechanics makes possible communication procedures and computational tasks that could outperform classical devices in terms of security or speed [1]. There are extensive experimental efforts in many fields to realize implementations of the necessary building blocks for quantum information processing. The key ingredient is an externally controlled evolution of a superposition state which implies a form of quantum parallelism. The alternatives range from electrons spins [2], superconducting circuits [3, 4], quantum electrodynamic cavities [5, 6], and optical ion traps [7], to nuclear magnetic resonance (NMR) in liquids [8] and solid state [9].

One of the most important building blocks is the swap gate, where a system jumps between two degenerated states,  $A$  and  $B$ , when the coupling  $V_{AB}$  is turned on. Starting on state  $A$ , the return probability oscillates with the Rabi frequency  $\omega_0 = 2V_{AB}/\hbar$ . However, it is clear that it is not feasible to isolate completely any real system. In practice, the interactions with an environment [10, 11] perturb the evolution, smoothly degrading the quantum interferences with a “decoherence” rate,  $1/\tau_\phi$ . This rate is usually identified with the system-environment (SE) interaction rate  $1/\tau_{SE}$ , typically evaluated from the Fermi Golden Rule (FGR). In spin systems,  $A$  and  $B$  could be the  $\uparrow\downarrow$  and  $\downarrow\uparrow$  spin configurations respectively. Weak interactions ( $1/\tau_{SE} \ll 2\omega_0$ ) produce a slightly slower oscillation which decays at a rate  $1/\tau_\phi = 1/(2\tau_{SE})$ . There are experimental conditions, however, where the observed frequency shows a dynamical transition on its dependence of the SE interaction [9]. In fact, the swapping frequency is a *non-analytic* function of the interaction rate. At a critical strength  $1/\tau_{SE}^c = 2\omega_0$ , the oscillation freezes indicating a *transition* to a new *dynamical regime*. The initial state now decays to equilibrium at a slower rate  $1/\tau_\phi \propto \omega_0^2 \tau_{SE}$ , which vanishes for strong SE interaction. This last regime can be seen as a Quantum Zeno phase, where the dynamics is inhibited by the frequent “observations” [12] of the environment. Such quantum freeze can arise as a pure dynamical process, governed by strictly unitary evolutions (see Ref. [13, 14]). Indeed, some of the phenomenology of that transition was not foreign to spectroscopists. The collapse of the independent resonance lines leads to the exchange and motional narrowing addressed by Van Vleck [15] and Bloembergen, Purcell and Pound [16] in the 40’s and synthesized in the analytic properties of a phenomenological classical probabilistic model by P. W. Anderson [17]. The quantum description of the phase transition [9] required a self-consistent calculation of the oscillation in presence of the SE interaction. While the system remembers its previous state, the environment was described in the “fast fluctuations” approximation where it has no memory of its previous state [18].

In this work we present a simple and exactly solvable quantum model that, while only describing the coherent part of a spin swap gate dynamics [19], presents the dynamical transitions. Our goal is to deepen in the understanding of how bath’s memory affects the system dynamics beyond the Fermi Golden Rule. A complementary vision for the dynamics under the action of a given Hamiltonian is, of course, the spectral representation which can be studied as function of the SE interaction strength. However, the energy representation hides much useful dynamical information in subtle spectral properties, such

us resonances that collapse at the "Exceptional Points" (EP) in the complex plane. Other unusual properties involve resonances that shrink and jump into the non-physical Riemann sheet to become virtual states. Ultimately, these resonances can transform themselves into isolated singularities on the real axis, accounting for localized states. In our model all of these transitions will appear naturally through the variation of a *single* control parameter. There are a number of physical systems that show some of these delicate spectral properties: The EP or collapse of resonances has been observed in crystals of light [20], electronic circuits [21], propagation of light in dissipative media [22, 23], vacuum Rabi splitting in semiconductor cavities [24], in microwave billiards [25, 26, 27, 28], and there are a number of examples drawn from electron-paramagnetic resonance [29], and solid state NMR [9]. It also appears in many theoretical models: e.g., describing the decay of superdeformed nuclei [30], phase transitions and avoided level crossings [31, 32, 33], geomagnetic polarity reversal [34], tunneling between quantum dots [35, 36], optical microcavity [37], vibrational surface modes [38], and in the context of the crossing of two Coulomb blockade resonances [39]. On the other hand, the Virtual-Localized transition has been addressed in the context of the famous  $n - p$  singlet system [40], models of stabilization of quantum mechanical binding by potential barriers [41], Feshbach resonances [42, 43], stability of atomic and molecular states [44, 45] and also in virtual bound states in photonic crystals [46].

This paper is organized as follows. In section II the model is presented. It is solved in Section III using a Green's function formalism [47] and its analytical properties are analyzed. In Section IV the different parametric regions are associated with the analytic properties of the density of states: Region I) collapsed resonances; Region II) resolved resonances; Region III) out of band resonances; Region IV) virtual states; and Region V) pure point spectrum. These parametric regions are associated with distinctive dynamical regimes: overdamped, damped oscillations, environment controlled quantum diffusion, anomalous diffusion and localized dynamics, respectively. The anomalous diffusion then could be considered as a signature of virtual states. The summarizing conclusions are presented in the last section.

## II. THE MODEL

Our model, schematized in Fig. 1, is a tight-binding semi-infinite linear chain. The Hamiltonian has one part that describes the two states of the system, another that describes

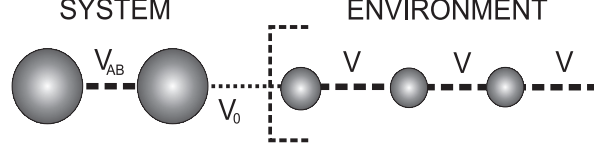


FIG. 1: Representation of the system and the environment. The first two sites are connected through  $V_{AB}$ . The hopping amplitude inside the environment is  $V$ . The system-environment interaction is  $V_0$ .

the infinite degrees of freedom of an environment and a third part that is the interaction between both. It is expressed as,

$$H = H_S + H_E + V_{SE}, \quad (1)$$

where,

$$H_S = E_A |A\rangle \langle A| + E_B |B\rangle \langle B| - V_{AB} (|A\rangle \langle B| + |B\rangle \langle A|) \quad (2)$$

$$H_E = \sum_{n=1}^{\infty} E_n |n\rangle \langle n| - V (|n\rangle \langle n+1| + |n+1\rangle \langle n|) \quad (3)$$

$$V_{SE} = -V_0 (|B\rangle \langle 1| + |1\rangle \langle B|), \quad (4)$$

and  $|n\rangle$ , with  $n \geq 1$ , is the state localized at the  $n$ -th site of the chain.  $V_{AB}$ ,  $V_0$  and  $V$  are the positive hopping amplitudes between two contiguous sites. The first two sites, linked by  $V_{AB}$ , are what we call *the System*. The rest of the chain is what we take as *the environment*. In this work, we are interested in the case  $E_A = E_B = E_n = 0$ . This choice of parameters produces a symmetric connection to the environment, enabling a rich spectrum.

This model applies to implementations of NMR quantum information processors by resorting to the Jordan-Wigner transformation [9][48] that maps spins into Fermionic interactions. More specifically, spin excitations in spin chains with XY interaction are transformed, at experimentally relevant high temperatures, into a single fermion in a tight binding chain [49]. In particular, Ref. [9] shows how the Swap Gate in solid state NMR, is mapped into the dynamics of our model plus an incoherent contribution. The fermionic model, having incorporated the temperature in the appropriate regime, is a natural alternative to the various spin-boson models, where a number of transitions are also known to exist as a function of temperature and interaction strength [50].

### III. ANALYTIC SOLUTION.

In this work we use the Green's Function (GF) formalism to solve the model. Starting with the isolated system  $H_S$ , we define the GF matrix  $\mathbb{G}$ ,

$$\mathbb{G}^{(0)}(\varepsilon) = (\mathbb{H}_S - \varepsilon \mathbb{I})^{-1}. \quad (5)$$

In order to make a fully consistent definition of  $G_{n,m}(\varepsilon)$  as the Fourier transform of the retarded propagator,  $G_{n,m}(t)$ , we assume that each site  $n$  has an intrinsic decay process  $E_n \rightarrow E_n - i\eta_n$ . This solves the Gutzwiller objection on this aspect [51]. However, since these imaginary parts are considered infinitesimal, they are not written explicitly in what follows.

The first diagonal component of  $\mathbb{G}(\varepsilon)$  gives us information about the system dynamics. This component becomes,

$$G_{AA}^{(0)}(\varepsilon) = \frac{1}{\varepsilon - \frac{V_{AB}^2}{\varepsilon}}. \quad (6)$$

Here, we can see that the poles of  $G_{AA}^{(0)}(\varepsilon)$  give the system energies,  $\tilde{E}_{A,B} = \pm V_{AB}$ . If we consider an isolated system of two sites, and excite the first one; the system evolves oscillating between the states  $|10\rangle$  and  $|01\rangle$  with a characteristic Rabi frequency  $\omega_0 = \frac{2V_{AB}}{\hbar}$ . This oscillation is used to generate a Swap Gate by letting the Hamiltonian act during a time  $t_{\text{swap}} = \frac{5\pi}{2} \frac{1}{\omega_0}$ .

When we take into account the environment, the first diagonal component of the GF becomes,

$$G_{AA}(\varepsilon) = \frac{1}{\varepsilon - \frac{V_{AB}^2}{\varepsilon - \frac{V_0^2}{V^2} \Sigma(\varepsilon)}}. \quad (7)$$

Typically the Self Energy  $\Sigma \simeq \Delta - i\Gamma$  is evaluated within a Fermi Golden Rule approximation [52] as an  $\varepsilon$  independent complex number. Since this would imply neglecting all dynamics and memory effects of the environment, such procedure could miss some subtle behaviors [53, 54, 55]. Our model enables the evaluation of the exact self-energy of an environment represented by the Semi-Infinite Chain, and hence accounts precisely for these “memory effects”. According to the continued fractions solution [47] of the Renormalized Perturbation

Expansion [56],

$$\Sigma(\varepsilon) = \frac{V^2}{\varepsilon - \frac{V^2}{\varepsilon - \frac{V^2}{\varepsilon - \dots}}} \quad (8)$$

$$= \frac{V^2}{\varepsilon - \Sigma(\varepsilon)}. \quad (9)$$

which sums up to the form:

$$\Sigma(\varepsilon) = \Delta(\varepsilon) - i\Gamma(\varepsilon), \quad (10)$$

with

$$\Delta(\varepsilon) = \begin{cases} \frac{\varepsilon}{2} - \sqrt{\left(\frac{\varepsilon}{2}\right)^2 - V^2} & \varepsilon > 2V \\ \frac{\varepsilon}{2} & |\varepsilon| \leq 2V \\ \frac{\varepsilon}{2} + \sqrt{\left(\frac{\varepsilon}{2}\right)^2 - V^2} & \varepsilon < -2V, \end{cases} \quad (11)$$

and

$$\Gamma(\varepsilon) = \begin{cases} 0 & \varepsilon > 2V \\ \sqrt{V^2 - \left(\frac{\varepsilon}{2}\right)^2} & |\varepsilon| \leq 2V \\ 0 & \varepsilon < -2V. \end{cases} \quad (12)$$

A brief commentary on the complex self-energies, i.e. non-Hermitian terms, is in order. Its appearance, either in a FGR calculation or in the exact solution of Eq. 9, relies on the fact that the new eigenstates are completely orthogonal to the unperturbed ones. In our case they are extended states enabled by taking the thermodynamic limit of an infinite number of states before  $\eta$  is enabled to reach 0 [57]. As discussed above, adding this small imaginary part means putting the system in contact with an additional environment. In this situation, Eq. 9 produces a self-energy containing a square root function of the energy instead of a ratio among polynomials that results when Eq. 8 is applied to a finite system. The sign in front of the square root in Eqs. 11 and 12 is chosen to ensure the physical (i.e. decaying) behavior when  $\eta < 0$ . As discussed in Ref. [57] the presence of non-Hermitian terms is fundamental in allowing a dynamical phase transition. In the general context of non-Hermitian quantum mechanics a similar conclusion holds [58].

The poles of Eq. 7, control the dynamics of the system and can be obtained analytically as,

$$\varepsilon_r^2 = \frac{V_{AB}^2 (2V^2 - V_0^2) - V_0^4 \pm V_0^2 \sqrt{(V_{AB}^2 + V_0^2)^2 - 4V_{AB}^2 V^2}}{2(V^2 - V_0^2)}. \quad (13)$$

Eq. 13 has four solutions, see Fig. 2. When they have an imaginary part, only the negative one represents a decaying response to an initial condition. This imaginary part is precisely the exponential decay rate in the Self-Consistent Fermi Golden Rule [59]. When the four poles are real, the physical ones approach to the isolated system poles shown with dashed lines. All poles are represented in Fig. 2. The real and imaginary part are shown as a function of the system hopping  $V_{AB}$  for fixed values of  $V_0 = 0.8V$ . The solutions not satisfying the above conditions are indicated with dotted lines. Hereafter, we will refer as “the Poles” of the GF only those indicated by the continuous line.

The Local Density of States (LDoS), can be evaluated as

$$N_A(\varepsilon) = -\frac{1}{\pi} \lim_{\eta \rightarrow 0^+} \text{Im } G_{AA}(\{E_n - i\eta_n\}_{\forall n}, \varepsilon). \quad (14)$$

This definition is equivalent to the standard one,  $-\frac{1}{\pi} \lim_{\eta \rightarrow 0^+} \text{Im } G_{AA}(\varepsilon + i\eta)$ , for most practical purposes.

An advantageous feature of the present model is that LDoS for  $|\varepsilon| \leq 2V$  can be factorized as

$$N_A(\varepsilon) = N_1(\varepsilon) \times L_1(\varepsilon) \times L_2(\varepsilon). \quad (15)$$

Here,  $L_1$  and  $L_2$ , are Lorentzian Functions (LFs), and  $N_1$  is the *density of directly connected states* (i.e. the LDoS of the first site of the semi infinite-chain).

$$N_1(\varepsilon) = \frac{1}{\pi V^2} \sqrt{V^2 - \frac{\varepsilon^2}{4}}. \quad (16)$$

The LF's  $L_1(\varepsilon)$  and  $L_2(\varepsilon)$  are related with the real and the imaginary part of the GF's poles. Their centers move with the real part of the poles, and their widths are determined by the imaginary part.

In Fig. 2 it is observed that there are regions with different analytical behaviors, some of them separated by abrupt changes that are consequence of the non-analytical points of the GF poles.

The difference between the physical poles has a real part,  $\tilde{\omega} = |\text{Re}(\varepsilon_{r1}) - \text{Re}(\varepsilon_{r2})| = 2|\text{Re}(\varepsilon_{r1})|$ , representing an effective Rabi frequency. The imaginary part is associated with

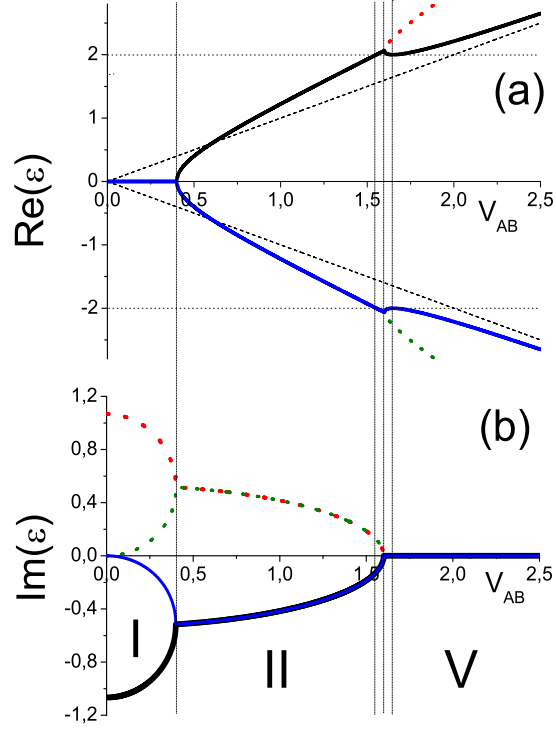


FIG. 2: (Color online) Real (a) and imaginary (b) part of the Green function poles vs.  $V_{AB}$  for  $V_0 = 0.8$ . All energies are in  $V$  units. a) the dashed line represent the poles for an isolated system. Different colors identify the poles. The non-physical ones are represented with dotted lines. The vertical dotted lines divide the dynamical regions.

the decay rate toward the environment. This work mainly focuses on the study of  $\tilde{\omega}$  behavior, as the parameter that characterizes the dynamics.

The relation between GF's analytic properties and the dynamics is clarified by writing the survival probability in the energy-time representation:

$$\begin{aligned}
 P_{AA}(t) &= \int_{-\infty}^{\infty} d\varepsilon \int_{-\infty}^{\infty} \frac{d\omega}{2\pi} G_{AA}(\varepsilon + \frac{1}{2}\hbar\omega) G_{AA}^*(\varepsilon - \frac{1}{2}\hbar\omega) \exp(-i\omega t) \\
 &= \left| \int_{-\infty}^{\infty} d\varepsilon N_A(\varepsilon) \exp(-i\varepsilon t/\hbar) \right|^2.
 \end{aligned} \tag{17}$$

This function measures the probability to find a particle in the site  $A$  at time  $t$ , provided that the system has had a particle at the same site at time  $t = 0$ . When the system is isolated,  $P_{AA}(t)$  oscillates with frequency  $\omega_0$ , which coincides with  $\tilde{\omega}$ . When the environment is taken into account  $P_{AA}(t)$  evolves in a more complex way. However, in spite of this complexity,



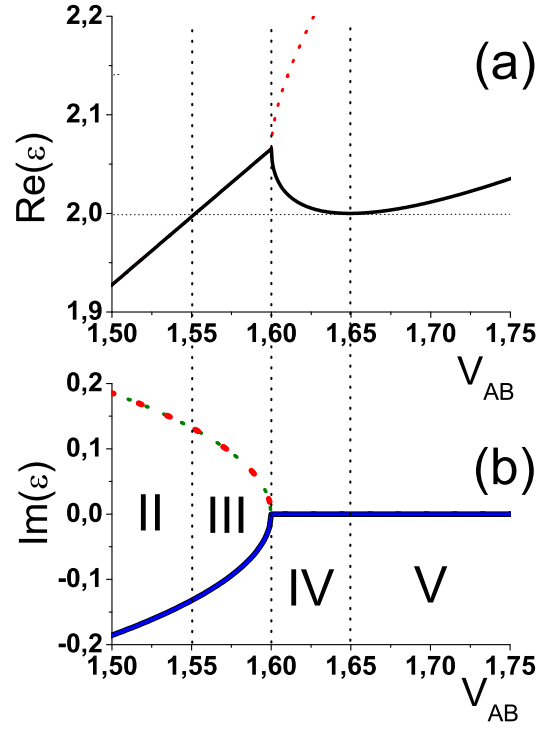


FIG. 3: (Color online) Zoom of Fig. 2 in the region where virtual states and out of band resonances occur.

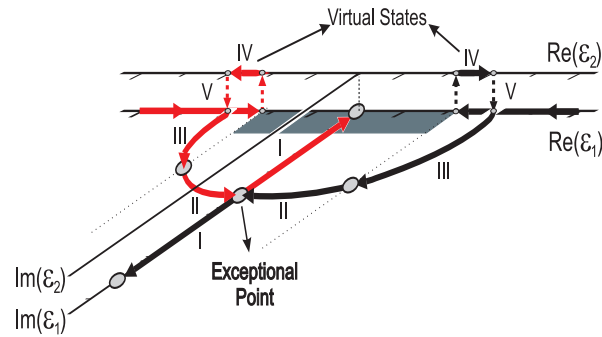


FIG. 4: (Color online) Paths of the two poles (Black and Red) of the GF as  $V_{AB}$  decreases. They go from the localized bonding and antibonding states into respective resonances that eventually collapse at the exceptional point. The bottom Riemann sheet contains the physical poles, while the upper sheet has the non-physical poles. The broader horizontal line in the center represents the continuous band of environment states. Notice that localized states transform into virtual states and out-of-band resonances before becoming well defined resonances.

the evolution at short times can be described by an exponentially decaying oscillation with frequency  $\tilde{\omega}$ .

In the next section we will present a deeper analysis of all spectral regions and their main dynamical characteristics.

#### IV. PARAMETRIC REGIONS

By analyzing the qualitative features of the Local Density of States (LDoS) as function of the control parameter  $V_{AB}$  we find five parametric regions separated by well defined critical values. We enumerate them from I to V as they are appearing by increasing  $V_{AB}$  and name them according to the main features in the LDoS and the behavior of the GF's poles in the complex plane. The most common situation occurs when the two states of the isolated system are mixed with the environment continuous and hence acquire a finite mean-life. This is Region II) of **Resolved Resonances**, a regime typically described by the FGR. When the interaction with the environment becomes strong enough, at the exceptional point appears the non trivial transition to Region I) of **Collapsed Resonances**. This is the regime where exchange narrowing occurs [17]. In the other extreme, we may consider that the internal interaction of the system is much stronger than the bandwidth of the environment's continuous spectrum. Hence, the system's bonding and anti-bonding states are pushed away from the band according to perturbation theory and they will remain localized. This is Region V) **Pure Point States**. Region III) **Out-of-Band Resonant States** and Region IV) **Virtual States**, would go almost unnoticed unless the internal and external interactions are very similar, see Fig. 5. In these cases the separation between system and environment becomes very delicate.

The main features of these regions can be identified by following the GF's poles into the complex plane as represented in Fig. 2 and zoomed in Fig. 3. We notice that poles in Region III and IV have a real part extending outside the band edges (indicated with an horizontal dotted line). However, as they enter region IV they loose their imaginary part. At this point the poles jump up to the second Riemann sheet, as represented in Fig. 4, and they become virtual states [41]. This is manifested in the fact they are poles of Eq. 7 using the unphysical branch of the self-energy. Hence, they do not show up as peaks or deltas in the density of states. Indeed, the LDoS given by Eq. 15 integrates to 1 within the band

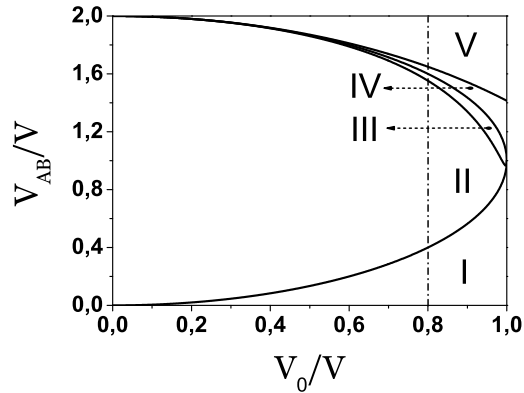


FIG. 5: Phase diagram of the different regimes as a function of  $V_{AB}/V$  and  $V_0/V$ . The vertical dash-dotted line represents the condition used in Figs. 2, 4, 6 and 7.

support. Only when the poles reach the band edge again, see Fig. 4, they return to the first Riemann sheet to become localized states.

Notice that if in Fig. 5 we move along the parameter space with a horizontal line, which means to keep  $V_{AB}$  constant, we are not going to see all the regions. At least one region would escape the analysis. From the experimental point of view this implies that it is preferable to vary the system frequency instead of the system environment interaction, in order to find all the regimes by controlling only one parameter. For that reason, hereafter in the plots we only vary the parameter  $V_{AB}$  while keeping  $V_0$  and  $V$  constant at 0.8 and 1 respectively.

In order to ensure consistency, we also studied the behavior of  $P_{AA}(t)$  by the exact diagonalization of the Hamiltonian of the finite system. In this case the environment size is taken large enough so the mesoscopic echoes do not show up at times of interest [59]. The evaluation of  $P_{AA}(t)$  allows us to univocally identify the localized states and the different decay laws of the other regimes. In the next sub-sections we will show, in more detail, the behavior of the system in each region.

#### A. Region I: Collapsed resonances (overdamped decay)

This region is found for:

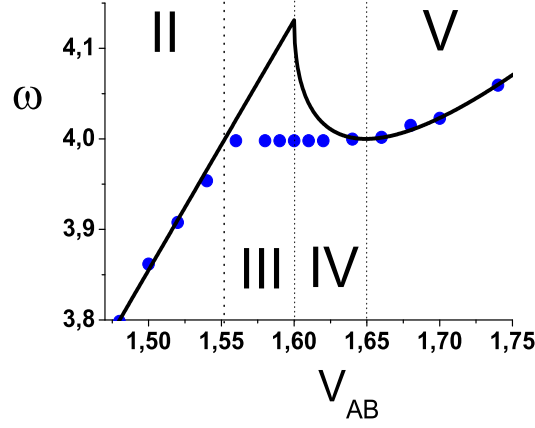


FIG. 6: (Color online) *Solid line*:  $\tilde{\omega}$  (poles effective frequency) vs.  $V_{AB}$ . *Blue dots*: effective frequency that fits the dynamics. The value for  $V_0$  is the same as in Fig.2.

$$|V_{AB}| < \left| V - (V^2 - V_0^2)^{1/2} \right|. \quad (18)$$

Under this condition,  $P_{AA}(t)$  decays exponentially and without oscillations until the survival collapse time [59]. At this moment the return amplitude from the environment starts to be comparable with the survival amplitude (see Fig. 7(I-b)). If we set  $V_0 = V$  we arrive to the case already treated in Ref. [59] where it is analyzed the decay of a surface spin excitation when it interacts with a spin chain.

The *real part* of both poles of the GF *coincide* with the site energy, which means that the effective frequency is zero. However, their respective *imaginary parts differ* substantially (see Fig. 4). One of them moves away from the real axis as the SE interaction increases while the other approaches the real axis. This means that one states is captured by the environment while the other becomes isolated by cause the Quantum Zeno Effect[9].

In this region  $L_1$  and  $L_2$  are two LF centered at 0, but with different widths,

$$L_{1,2}(\varepsilon) = C \frac{2\Gamma_{1,2}}{\varepsilon^2 + \Gamma_{1,2}^2}, \quad (19)$$

where,

$$C^2 = \frac{V_0^2 V_{AB}^2}{4\Gamma_1 \Gamma_2} \quad (20)$$

$$\Gamma_{1,2}^2 = \frac{V_0^4 - V_{AB}^2 (2V^2 - V_0^2)}{2(V^2 - V_0^2)} \mp \frac{\sqrt{(V_0^4 - V_{AB}^2 (2V^2 - V_0^2))^2 - 4V^2 V_{AB}^4 (V^2 - V_0^2)}}{2(V^2 - V_0^2)}. \quad (21)$$

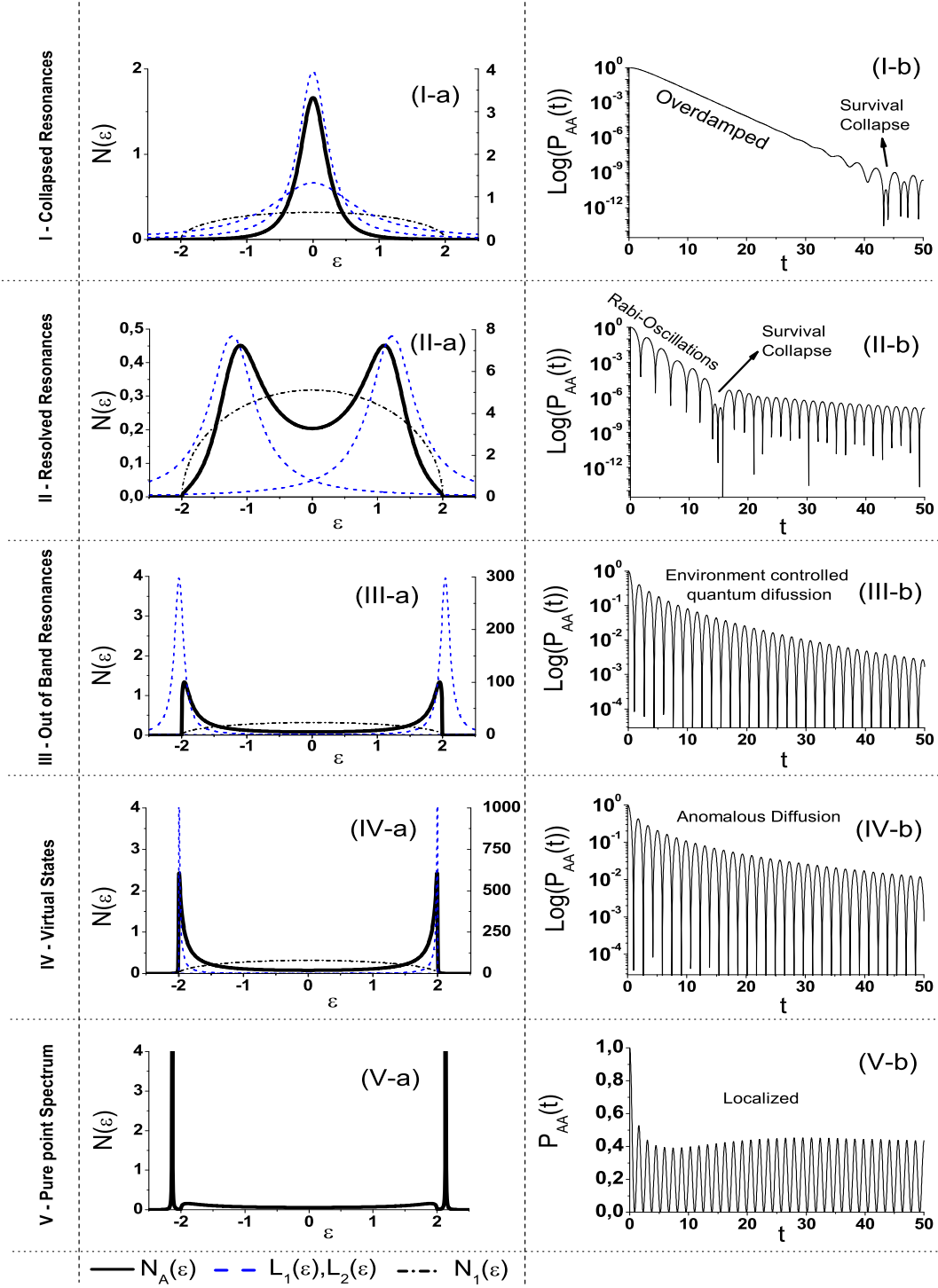


FIG. 7: (Color online) **(a)-Left side panels:** Black solid line: LDoS for the different regions [  $V_{AB} = 0.35$  (I), 1.0(II), 1.58 (III), 1.62 (IV) and 1.9 (V)]. Blue dotted line:  $L_1(\epsilon)$  and  $L_2(\epsilon)$ . Black Dash-Dotted line:  $N_1(\epsilon)$ . The right side scale corresponds to the  $L_1$  and  $L_2$  plots. **(b)-Right side panels:** Survival probability  $P_{AA}(t)$  in logarithmic scale except for (V-b), which is in normal scale.

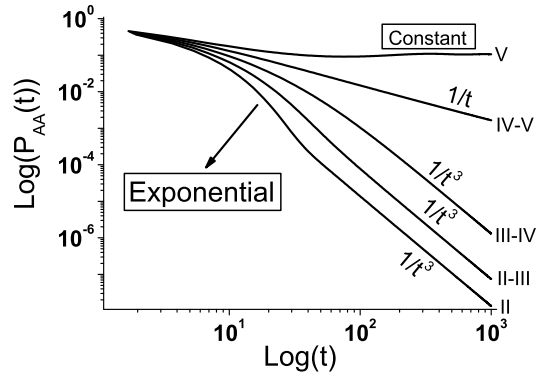


FIG. 8: Local dynamics in Log-Log scale for different regimes. The curve II and V represent evolutions inside the region II and V respectively. Curves II-III, III-IV and IV-V represent the survival probability at the transitions between regimes.

Fig. 7(I-a) shows the behavior of  $N_A$ ,  $N_1$  and the Lorentzians functions:  $L_1$  and  $L_2$ . The centers and the linewidth of  $L_1(\varepsilon)$  and  $L_2(\varepsilon)$  are exactly equal to the real and imaginary part of the poles of the GF respectively.

When  $V_{AB}$  reaches zero,  $\Gamma_1$  vanishes, which is consistent with the fact that the first site becomes completely isolated and the second site behaves exactly as the case treated in Ref. [59]. On the other hand at the value  $V_{AB} = \left| V - (V^2 - V_0^2)^{1/2} \right|$  the system presents an EP. In this point both Lorentzians are equal and beyond this point  $\tilde{\omega}$  starts to grow up (see Fig. 2). This kind of behavior was observed previously for different physical systems [9, 20, 21, 22, 23, 24, 25, 26, 27, 28, 60]. In our case, we can interpret this as a change of model from one with two sites interacting with an environment, to other with only one surface site coupled to a semi-infinite chain.

### B. Region II: Resolved Resonances (damped oscillations)

This regime occurs for values of  $V_{AB}$  satisfying:

$$\left| V - (V^2 - V_0^2)^{1/2} \right| < |V_{AB}| < \left| \sqrt{\left( 1 + 16 \frac{V^2}{V_0^4} (V^2 - V_0^2) \right) \left( (2V^2 - V_0^2) - 2\sqrt{V^2 (V^2 - V_0^2)} \right)} \right|. \quad (22)$$

This parametric region is characterized by the oscillatory-exponential decay of  $P_{AA}(t)$  at short times, Figs. 7(II-b), followed by a quantum diffusive regime ( $t^{-3}$ ) that is better appreciated in Fig. 8. The power law decay is consequence of the environment memory effects and corresponds to quantum diffusion from a  $d$ -edge. This is verified by making a Fourier Transform of a LDoS of the form  $N_1(\varepsilon) \propto \varepsilon^\nu \theta[\varepsilon]$  which leads to a survival probability of the asymptotic form  $P(t) \sim t^{-(2\nu+2)}$ . In a *bulk* of  $d$  dimensions  $\nu = d_{\text{eff.}}/2 - 1$  with  $d_{\text{eff.}} = d$ . Notably, our case corresponds to a survival probability of a state in a *surface* or *edge*. This one decays as being in a higher effective dimension,  $d_{\text{eff.}} = d + 2n$  with  $n \leq d$  the order of the surface. In our case  $n = d = 1$ .

The poles in this region have both real and imaginary parts. At short times, the real part controls the oscillatory behavior ( $\tilde{\omega} = 2\text{Re}(\varepsilon)$ ) and the imaginary part determines the rate of the exponential decay. On the other hand, at long times the excitation decays with a  $t^{-3}$  law and oscillates with a frequency determined by the environment band width  $4V$ .

Here, the critical time  $t_c$  is the time scale at which the quantum pathways returning from the environment starts to be comparable to the pure survival amplitude. Hence,  $t_c$ , which decreases with  $V_{AB}$ , divides the exponential decay from the diffusive decay.

The LDoS can be expressed in the same way as Eq. 15, but in this regime the LF are centered at symmetric points and have the same width (see Fig. 7(II-a)),

$$L_{1,2}(\varepsilon) = C \frac{2\Gamma}{(\varepsilon \mp \varepsilon_r)^2 + \Gamma^2}, \quad (23)$$

with,

$$C^2 = \frac{V_0^2 V_{AB}^2}{4\Gamma^2} \quad (24)$$

$$\Gamma^2 = \frac{V_0^4 - V_{AB}^2(2V^2 - V_0^2)}{4(V^2 - V_0^2)} + \sqrt{\frac{V^2 V_{AB}^4}{4(V^2 - V_0^2)}} \quad (25)$$

$$\varepsilon_r^2 = \frac{V_{AB}^2(2V^2 - V_0^2) - V_0^4}{2(V^2 - V_0^2)} + \Gamma^2. \quad (26)$$

It is interesting to notice that the Rabi frequency could either be slower than the unperturbed one, when  $V_{AB} \ll V$ , or faster, when  $V_{AB} \gtrsim V$ . The precise cross over results from Eq.26 when  $\varepsilon_r = V_{AB}$ .

### C. Region III: Out-of-Band Resonances (environment controlled quantum diffusion).

This region is found for  $V_{AB}$  satisfying:

$$\left| \sqrt{\left(1 + 16 \frac{V^2}{V_0^4} (V^2 - V_0^2)\right) \left((2V^2 - V_0^2) - 2\sqrt{V^2 (V^2 - V_0^2)}\right)} \right| < |V_{AB}| < \left| V + (V^2 - V_0^2)^{1/2} \right|. \quad (27)$$

If we only take into account the poles of the GF the system resembles the Resolved Resonances regime. However, if we compare their LDoS and  $P_{AA}(t)$ , we conclude that this is a new regime.

In this region, it is no longer possible to distinguish an exponential decay in  $P_{AA}(t)$  (see Fig. 7(III-b)). This is because the time  $t_c$  is too short. This implies that the oscillations are a direct consequence of the environment. In Fig. 6 it is observed that the frequency obtained directly from the numerical solutions remains constant at  $4V$  while  $\tilde{\omega}$  (poles effective frequency) continues growing, confirming our analysis.

The expression for the LDoS presented in Eq. 15 is still valid, but the LF are centered outside the band edges (see Fig. 7(III-a)). If we analyze the dynamics in term of the LDoS, we see that the tails of the LF decay as  $\varepsilon^{-2}$ , which means that the LDoS will have a Van Hove singularity as  $\varepsilon^{1/2} \times \varepsilon^{-2}$ , which implies that the local excitation will decay as  $t^{-3}$  at long times (see Figs. 7(III-b) and 8).

### D. Region IV: Virtual States (anomalous diffusion)

This region corresponds to the range,

$$\left| V + (V^2 - V_0^2)^{1/2} \right| < |V_{AB}| < \sqrt{2(2V^2 - V_0^2)}. \quad (28)$$

The poles in this region do not have imaginary part. For this reason it might be expected that poles were localized states[56]. However, both the LDoS of Fig. 7(IV-a) and the dynamics shown in Fig. 7(IV-b) and Fig. 8 probes that this is not the case. The reason is that the poles had moved to a second Riemann sheet [41, 42] (see Fig. 4). In such case only the use of the unphysical sign of the self-energy could provide poles. The dynamics in this regime presents a striking transition between a  $t^{-3}$  decay (at  $V_{AB} = \left| V + (V^2 - V_0^2)^{1/2} \right|$ ) to a  $t^{-1}$  behavior (at  $V_{AB} = \sqrt{2(2V^2 - V_0^2)}$ ). This is shown in Fig. 8.



Once again, we can express the LDoS as in Eq. 15, however its interpretation is different. In this region  $\varepsilon_r$  is still outside the band edges and yet the value of  $\Gamma$  becomes imaginary. The fact that  $\Gamma$  is transformed into an imaginary number implies that  $L_1$  and  $L_2$  are no longer LF. If we now analyze the tails of these functions, we observe that they decay as  $\varepsilon^{-1}$ . This leads to a LDoS with a Van Hove singularity of the form  $\varepsilon^{1/2} \times \varepsilon^{-1}$ . Therefore, we can achieve a  $t^{-1}$  behavior of  $P_{AA}$  at long times. This fact is indeed confirmed by the observed dynamics (see Fig. 8). As in the previously analyzed section,  $\tilde{\omega}$  do not follows the observed oscillation frequency (see Fig. 6 and 7(IV-a)). Instead, it is fixed by the environment band width  $4V$ .

When  $V_{AB}$  reaches the value  $\sqrt{2(2V^2 - V_0^2)}$ , there is a change in the nature of the Van Hove singularities from  $\varepsilon^{\frac{1}{2}}$  to  $\varepsilon^{-\frac{1}{2}}$ . Consequently,  $P_{AA}(t)$  decays exactly as a  $t^{-1}$  (see Fig. 8). From this point on, the states become localized.

It is interesting to note that while the presence of the virtual states is not clearly distinguishable in the observable LDoS, the anomalous diffusion, where  $P_{AA}(t)$  moves gradually between  $t^{-3}$  and  $t^{-1}$ , should enable its experimental identification.

### E. Region V: Pure Point States (localized)

Finally, the last region appears when,

$$|V_{AB}| > \sqrt{2(2V^2 - V_0^2)}. \quad (29)$$

Two localized states emerge from the band edges as shown in Fig. 7(V-a). The poles are real. Fig. 6 shows that  $\tilde{\omega}$  recovers its interpretation as the effective system frequency. In this region the environment renormalization is almost negligible and its only effect is to slightly correct the value of the effective frequency. If  $V_{AB}$  becomes large enough  $\tilde{\omega}$  reaches  $\omega_0$ .

The dynamics in this region, Fig. 7(V-b) is characterized by an oscillatory  $P_{AA}(t)$  that only decays at very short times, after which the amplitude of the oscillation remains constant.

## V. CONCLUDING REMARKS

By considering an exactly solvable model for a swap gate in presence of an environment, we discussed how the bath's memory affects the dynamics when treated beyond the Fermi

Golden Rule. The unperturbed Rabi frequency sweep through different dynamical and analytic regimes when moving continuously a single parameter.

We have shown that depending on the value of the internal time scales of the system, the environment can induce multiple phase transitions in the system dynamics. Our model shows uncommon regimes as the exchange narrowing starting at the Exceptional Point and the Virtual States by moving a single parameter. The fact that all the dynamical phases appear in the same system, offered the opportunity to study the transitions between them and hence to determine the precise points where the transition occurs. Through the dynamics, we have characterized the difference between collapsed resonances, resolved resonances, out-of-band resonances, virtual states and the pure point states. In particular, we have shown that in the virtual state regime there is an anomalous quantum diffusive law, which at long times is observed as a change in the decay law from  $t^{-3}$  to  $t^{-1}$ . We have found an expression for the LDoS which explicit the presence of the resonances. This LDoS is factorized in three terms. A density of directly connected states ( i.e. the LDoS at the environment's surface) and two Lorentzian Functions whose widths become imaginary in the virtual state regime. The edges of the LDoS determine the behavior at long times. It is then clear that the anomalous diffusion is related to the fact that the Van Hove singularities at these edges are modified. This change occurs when the Lorentzian widths become imaginary.

Note that the complexity of the dynamics for this relatively simple system, emerges as a consequence of the explicit way in which the environment is modeled. Details like Out-of-band Resonant States and Virtual States could not have been observed in simpler representations of the environment as the usual broad-band or the self-consistent Born approximations. The results of our model system shows that a zero imaginary part of the poles is not enough as a localization criteria [56]. In particular, virtual states have zero imaginary part, but any local excitation in this parametric regime shows a complete decay to the environment.

Another parameter that characterizes the dynamics, is the oscillation frequency. First, in the Region I (collapsed resonances), before the system reaches the EP, there is an over-damped decay as expected. When the unperturbed Rabi frequency  $\omega_0$  exceeds the critical value, at the EP, the resonances become resolved (Region II).  $P_{AA}(t)$  show an exponentially attenuated oscillation with a frequency  $\tilde{\omega}$  given by the poles difference. This frequency,  $\tilde{\omega}$ , goes from 0, at the EP, to a value higher than  $\omega_0$ . In the region III (out-of-band resonances)

and IV (virtual states) the observed frequency is fully determined by the environment bandwidth and not by the GF poles, while the decay follows different power laws. These are particularly stable regimes for a swap gate since the effective Rabi frequency does not depend on the internal parameter. Further increase of  $\omega_0$  leads to Region V of localized states where the observed frequency is always higher than  $\omega_0$  but tends to it as  $V_{AB} \rightarrow \infty$ .

An interesting message that we can extract from the phase diagram of Fig. 5 is that by changing  $V_{AB}/V$  one can always move between all five regimes. However, for small values of the interaction with the environment ( $V_0/V$ ) the transition to localized states occurs within a very small range of  $V_{AB}/V$  and hence most chances are that it goes unobserved. The diagram indicates that a clear numerical or experimental observation of the full dynamical wealth would only be possible for  $V_0/V \lesssim 1$ .

As a final remark, we again mention that because of its simplicity, our model can be arranged to describe various physical systems such as spin chains [9], microwave devices [61], arrays of tunneling coupled optical waveguides [62], periodic elastic arrays [63], or acoustic time reversal cavities [64]. Reciprocally, most of them should present the variate dynamical phenomena discussed here, provided that one focuses in the proper parameter range. These examples also suggest possible experimental setups where the parameters found in this work can be used as a knob enabling to store and exchange energy.

## VI. ACKNOWLEDGMENTS

The authors acknowledge Gonzalo Alvarez, Hernán Calvo, Ernesto Danieli and Elena Rufeil Fiori for sharing their experiences in related fields. Patricia Levstein and Pablo Serra helped with discussions and useful references. HMP acknowledges hospitality of MPI-PKS and Abdus Salam ICTP where discussion with Ingrid Rotter and Maksim Miski-Oglu helped to enrich this work. The work was made possible through the financial support from CONICET, ANPCyT and SeCyT-UNC.

- 
- [1] Charles H. Bennett and David P. DiVincenzo, *Nature* **404**, 247 (2000).
  - [2] F. H. L. Koppens, C. Buizert, K. J. Tielrooij, I. T. Vink, K. C. Nowack, T. Meunier, L. P. Kouwenhoven and L. M. K. Vandersypen, *Nature* **442**, 766 (2006).|

- [3] D. Vion, A. Aassime, A. Cottet, P. Joyez, H. Pothier, C. Urbina, D. Esteve, M. H. Devoret, *Science* **296**, 5569 (2002).
- [4] Y. Nakamura, Yu. A. Pashkin and J. S. Tsai, *Nature* **398**, 786 (1999).
- [5] A. Wallraff, D. I. Schuster, A. Blais, L. Frunzio, R.-S. Huang, J. Majer, S. Kumar, S. M. Girvin, and R. J. Schoelkopf, *Nature (London)* **431**, 162 (2004).
- [6] J. M. Raimond, M. Brune, and S. Haroche, *Rev. Mod. Phys.* **73**, 565 (2001).
- [7] F. Schmidt-Kaler, H. Häffner, M. Riebe, S. Gulde, G. P. T. Lancaster, T. Deuschle, C. Becher, C. F. Roos, J. Eschner and R. Blatt, *Nature* **422**, 408 (2003).
- [8] C. Ramanathan, N. Boulant, Z. Chen, D. G. Cory, Isaac C. and M. Steffen, *Quantum Information Processing* **3**, 1 (2004).
- [9] G. A. Álvarez, E. P. Danieli, P. R. Levstein, and H. M. Pastawski, *J. Chem. Phys.* **124**, 1 (2006).
- [10] W. H. Zurek, *Rev. Mod. Phys.* **75**, 715 (2003); W. H. Zurek, F. M. Cucchietti and J. P. Paz, *Acta Physica Polonica B* **38**, 1685 (2007).
- [11] C. J. Myatt, B. E. King, Q. A. Turchette, C. A. Sackett, D. Kielpinski, W. M. Itano, C. Monroe, D. J. Wineland, *Nature* **403**, 269 (2000).
- [12] B. Misra and E. C. G. Sudarshan, *J. Math. Phys.* **18**, 756 (1977).
- [13] S. Pascazio and M. Namiki, *Phys. Rev. A* **50** 4582 (1994).
- [14] H. M. Pastawski and G. Usaj, *Phys. Rev. B* **57**, 5017 (1998).
- [15] J. H. Van Vleck, *Phys. Rev.* **74**, 1168 (1948).
- [16] N. Bloembergen, E. M. Purcell and R. V. Pound, *Phys. Rev.* **73**, 679 (1948).
- [17] P. W. Anderson, *J. Phys. Soc. Jpn.* **9**, 316 (1954).
- [18] G. A. Álvarez, E. P. Danieli, P. R. Levstein, and H. M. Pastawski, *Phys. Rev. A* **75**, 062116 (2007).
- [19] E. P. Danieli, H. M. Pastawski, and G. A. Álvarez, *Chem. Phys. Lett.* **402**, 88 (2005).
- [20] M. K. Oberthaler, R. Abfalterer, S. Bernet, J. Schmiedmayer and A. Zeilinger, *Phys. Rev. Lett.* **77**, 4980 (1996).
- [21] T. Stehmann, W. D. Heiss, and F. G. Scholtz, *J. Phys. A* **37**, 7813 (2004).
- [22] A. L. Shuvalov and N. H. Scott, *Acta Mech.* **140**, 1 (2000).
- [23] M. V. Berry and M. R. Dennis, *Proc. R. Soc. London, Ser. A* **459**, 1261 (2003).
- [24] G. Khitrova, H. M. Gibbs, M. Kira, S. W. Koch and A. Scherer, *Nature Phys.* **2**, 81 (2006).

- [25] C. Dembowski, H. D. Gräf, H. L. Harney, A. Heine, W. D. Heiss, H. Rehfeld and A. Richter, Phys. Rev. Lett. **86**, 787 (2001).
- [26] B. Dietz, T. Friedrich, J. Metz, M. Miski-Oglu, A. Richter, F. Schäfer and C. A. Stafford, Phys. Rev. E **75**, 027201 (2007).
- [27] C. Dembowski, B. Dietz, H. D. Gräf, H. L. Harney, A. Heine, W. D. Heiss and A. Richter, Phys. Rev. E **69**, 056216 (2004).
- [28] C. Dembowski, B. Dietz, H. D. Gräf, H. L. Harney, A. Heine, W. D. Heiss and A. Richter, Phys. Rev. Lett. **90**, 034101 (2003).
- [29] L. M. B. Napolitano, O. R. Nascimento, S. Cabaleiro, J. Castro and R. Calvo, Phys. Rev. B **77**, 214423 (2008); A. J. Costa-Filho, C. E. Munte, C. Barberato, E. E. Castellano, M. P. D. Mattioli, R. Calvo, and O. R. Nascimento, Inorg. Chem. **38**, 4413 (1999); Rafael Calvo, Appl. Magn. Reson. **31**, 271 (2007), and references therein.
- [30] C. A. Stafford and B. R. Barrett, Phys. Rev. C **60**, 051305(R) (1999).
- [31] W. D. Heiss and A. L. Sannino, Phys. Rev. A **43**, 4159 (1991).
- [32] F. Keck, H. J. Korsch, and S. Mossmann, J. Phys. A **36**, 2125 (2003).
- [33] W. D. Heiss, Phys. Rev. E **61**, 929 (2000).
- [34] F. Stefani and G. Gerbeth, Phys. Rev. Lett. **94**, 184506 (2005).
- [35] D. M. Cardamone, C. A. Stafford, and B. R. Barrett, Phys. Stat. Sol. B **230**, 419 (2002).
- [36] E. P. Danieli, G.A. Álvarez, P. R. Levstein and H. M. Pastawski, Sol. St. Comm. **141**, 422 (2007).
- [37] S. Longhi, Phys. Rev. A **74**, 063826 (2006).
- [38] Hernán L. Calvo, and H. M. Pastawski, Braz. J. Phys. **36**, 963 (2006).
- [39] H. A. Weidenmüller, Phys. Rev. B **68**, 125326 (2003).
- [40] J. R. Taylor, *Scattering Theory: The Quantum Theory of Non-Relativistic Collisions*, Dover, (Mineola, 2000) p. 246.
- [41] H. Hogreve, Phys. Lett. A **201**, 111 (1995).
- [42] B. Marcellis, E. G. M. van Kempen, B. J. Verhaar and S. J. J. M. F. Kokkelmans, Phys. Rev. A **70**, 012701 (2004).
- [43] A. M. Pupasov, B. F. Samsonov and J.-M. Sparenberg, Phys. Rev. A **77**, 012724 (2008).
- [44] P. Serra, S. Kais and N. Moiseyev, Phys. Rev. A **64**, 062502 (2001).
- [45] M. T. Yamashita, T. Frederico, A. Delfino and Lauro Tomio, Phys. Rev. A **66**, 052702 (2002).

- [46] J. Inoue and K. Ohtaka, J. of Luminescence **108**, 251 (2004).
- [47] Horacio M. Pastawski and Ernesto Medina, Rev. Mex. Fis. **47**, 1 (2001) cond-mat/0103219.
- [48] E. Danieli, H. Pastawski and P. Levstein, Chem. Phys. Lett. **348**, 306 (2004).
- [49] Z. L. Mádi, B. Brutscher, T. Schulte-Herbrüggen, R. Brüschweiler and R. R. previous Ernst, Chem. Phys. Lett. **268**, 300 (1997).
- [50] S. Chakravarty and A. J. Leggett, Phys. Rev. Lett. **52**, 5 (1984).
- [51] M. C. Gutzwiller, in *Chaos and Quantum Physics*, edited by M.-J. Giannoni, A. Voros, and J. Zinn-Justin (North-Holland, Amsterdam, 1991).
- [52] Paolo Facchi and Saverio Pascazio, *La Regola d'Oro di Fermi*, Bibliopolis, (Napoli, 1999).
- [53] L. Khal'fin, Sov. Phys. JETP **6**, 1053 (1958).
- [54] L. Fonda, G.C. Ghirardi, A. Rimini, Rep. Prog. Phys. **41**, 588 (1978).
- [55] G. García-Calderón, J. L. Mateos and M. Moshinsky, Phys. Rev. Lett. **74**, 337 (1995).
- [56] E. N. Economou, *Green's Functions in Quantum Physics*, 3rd Ed. Springer, (Heidelberg, 2006).
- [57] H. M. Pastawski, Physica B **398**, 278 (2007).
- [58] E. Narevicius, P. Serra and N. Moiseyev, Europhys. Lett. **62**, 789 (2003).
- [59] E. Rufeil Fiori and H. M. Pastawski, Chem. Phys. Lett. **420**, 35 (2006).
- [60] M. Müller, F. M. Dittes, W. Iskra and I. Rotter, Phys. Rev. E **52**, 5961 (1995).
- [61] Luke A. Sweatlock, Stefan A. Maier and Harry A. Atwater, Proceedings of Electronic Components and Technology Conference (2003).
- [62] S. Longhi, Phys. Rev. Lett. **97**, 110402 (2006).
- [63] L. Gutiérrez, A. Díaz-de-Anda, J. Flores, R. A. Méndez-Sánchez, G. Monsivais and A. Morales, Phys. Rev. Lett. **97**, 114301 (2006).
- [64] Hernán L. Calvo, Ernesto P. Danieli, Horacio M. Pastawski, Physica B **398**, 317 (2007).